Fiducial-based monocular 3D displacement measurement of breakwater armour unit models

R. Vieira[†], *F. van den Bergh*[†], *B.J. van Wyk*[‡]

[†]Meraka Institute
CSIR, PO Box 395, Pretoria
South Africa, 0001
{rvieira, fvdbergh}@csir.co.za

[‡]French South African Technical Institute of Electronics
Tshwane University of Technology, Pretoria
South Africa, 0001
vanwykb@tut.ac.za

Abstract

This paper presents a fiducial-based approach to monitoring the movement of breakwater armour units in a model hall environment. Target symbols with known dimensions are attached to the physical models, allowing the recovery of three-dimensional positional information using only a single camera. The before-change and after-change fiducial positions are matched optimally, allowing the recovery of three-dimensional movement vectors representing the shifts in the positions of the physical models. Experimental results show that sub-millimeter accuracies are possible using 6-megapixel images of an A4-scale scene.

1. Introduction

Most harbours are occasionally subjected to storms powerful enough to damage infrastructure and ships, unless some preventative measures are taken. To protect the harbour infrastructure, arrays of armour units are used to absorb wave energy and reduce overtopping. The armour unit arrays must dissipate as much energy as possible, without deforming or suffering damage to the armour units themselves. This can be achieved by using armour units with an interlocking structure, such as the *dolos*, invented in East London in the 1963 [1].

Currently, the most effective method of validating the design of armoured breakwater structures is by building and evaluating physical scale models. A scale model of an entire harbour is constructed, complete with a sea floor modelled from bathymetry data. Wave generators are used to simulate wave conditions corresponding to 1000-, 100-, and 50-year storms. A successful armoured breakwater design will suffer little or no damage, measured in the model hall by assessing the magnitude of shifts in the positions of the scale model armour units. The CSIR's model hall facility, located in Stellenbosch, routinely conducts tests of this nature. Owing to the time-consuming nature of the physical modelling process, efforts are under way to develop computer simulations to assist with the validation of harbour designs [2].

Although physical models are considered to be an effective method of determining the stability of an armoured breakwater structure, the method used to evaluate the impact of simulated storm conditions is often subjective. Current methods of assessing damage to a breakwater include a visual comparison of a pair of before-simulation and after-simulation images. By displaying the *before* and *after* images in rapid succession, the changed regions of the scene appear to flicker — this technique is often referred to as *flicker animation* [3]. An operator will manually draw lines, representing movement vectors, on top of the flicker animation. A final assessment of the degree of damage that a breakwater structure has suffered during a simulation can then be estimated from the number and magnitude of the displacement vectors.

In addition to the subjective nature of the flicker technique measurements, they are inherently restricted to two dimensions. One potential method of improving the accuracy of the measurement of the movement of armour unit models is to attach accelerometers to the physical models. This, however, may restrict the movement of the models, and could become prohibitively expensive for larger tests involving many hundreds of armour units.

This paper proposes a different, cost effective method of measuring the movement of armour units using monocular machine vision techniques. Printed fiducial patterns are attached to the physical scale models, enabling an automated system to track the three-dimensional displacement of the models with millimeter accuracy.

Section 2 briefly discusses some recent applications of fiducials, followed by a description of the proposed system in Section 3. An empirical analysis of the positional accuracy of the system is presented in Section 4. Section 5 discusses how the fiducial method has been applied to compute the displacement of armour unit models, followed by some suggestions for future research in Section 6.

2. Background

2.1. Fiducial patterns

Fiducials are special geometric patterns that are used as reference points in machine vision systems. They have long been used in applications such as printed circuit board alignment, but have recently gained popularity in *augmented reality* applications. In these applications, the fiducials are used to define navigation reference points in a three-dimensional space; for example, Naimark and Foxlin demonstrated the use of fiducial patterns to mark up entire buildings [4].

The intended application of a fiducial has a significant impact on its design: some fiducials patterns are optimised to have a very large number of codes, while others are designed to provide very high positional accuracy. Some of the earlier applications in circuit alignment relied on very simple fiducial patterns such as squares, diamonds or circles. Owing to their simplicity, these fiducials could not encode a large number of different codes, but they were simple to detect. Amongst these early fiducials, Bose and Amir showed that circular fiducials produced significantly smaller positional errors compared to squares or

diamonds [5].

Owen *et al.* proposed a square fiducial based on Discrete Cosine Transform (DCT) basis images [6]. The fiducial is identified by a square black border surrounding the DCT-coded interior. The interior of the fiducial is represented as a 16×16 block, meaning that under ideal conditions, the fiducial can still be identified when the sampled image of the fiducial is only around 16×16 pixels in size. The advantage of the DCT-coded interior is that it provides a medium-sized coding space of around 200 codes, while maintaining robustness to noise. Another augmented reality fiducial system built around square patterns was proposed by Rekimoto and Ayatsuka [7]. Their CyberCode fiducial pattern more closely resembles a 2D barcode, and can encode 24 bits of information, after error correction. Unfortunately, Rekimoto and Ayatsuka do not elaborate on the minimum image size required or maximum viewing angle allowed for successful identification.

Despite the success of such square-based fiducial patterns, the circular patterns remain popular. Recent examples include the code proposed by Naimark and Foxlin, which can encode $2^{15} = 32768$ different codes [4]. The minimum image size required for successful fiducial identification reported by Naimark and Foxlin was 16×16 pixels; no figures were reported on the maximum allowed viewing angle. Another circular fiducial was proposed by López de Ipiña *et al.* for use in their TRIP location system [8]. The TRIP code consists of a "bull's eye" pattern in the centre, which is used to identify potential fiducials in the image. Two concentric tracks surround the central bull's eye, in which a sector-based scheme with three discrete sector sizes is used to encode the code value of a fiducial. This design allows for up to $3^9 - 1 = 19682$ different code values. López de Ipiña *et al.* report that the fiducials can be successfully identified provided that the pattern is at least 35×35 pixels in size, and the angle between the viewing direction and the surface normal is less than 70°.

2.2. Correspondence problem

The correspondence problem can be defined as the problem of finding the optimal association between two sets of features, allowing for the possibility that either set may contain elements that have no corresponding element in the other set. To calculate the movement vectors of fiducial patterns from a before- and after-simulation image pair, a similar correspondence problem arises: Given a fiducial pattern in the *before*-simulation image, find the most likely matching fiducial pattern in the *after*-simulation image.

In the simplest case, where only a single fiducial code pattern is attached to all the armour unit models, this would reduce to the problem of finding the closest point P_j (corresponding to the centroid of a fiducial pattern) in the *after* image corresponding to the point P_i in the *before* image. If more than one fiducial code is used, then this problem is constrained so that points may only be matched if their codes agree.

A simple algorithm that could be used to solve this type of correspondence problem is the Iterated Closest Point (ICP) method [9]. This algorithm computes the distances between all points, keeping only distances below a specified threshold. After rejecting outliers, a rigid motion transform is then computed on the remaining points. The algorithm iterates these steps until convergence. After the two sets have been aligned with the transform, the closest point pairs could be used as the correspondence map.

A more robust method was introduced by Maciel and Costeira [10]. Consider that the mapping of points in set $\mathbf{X}$ onto the points in set $\mathbf{Y}$ can be represented as a *partial permutation matrix* $\mathbf{P}$. This matrix resembles an identity matrix, with some of its rows exchanged, and potentially with some of the rows or columns set to zero. Finding the best mapping between $\mathbf{X}$ and $\mathbf{Y}$ can then be expressed as

$$\mathbf{P}^* = \arg\min_{\mathbf{P}} J(\mathbf{X}, \mathbf{Y}, \mathbf{P}) \quad s.t.\ \mathbf{P} \in \mathcal{P}_p(p_1, p_2).$$

where J represents a metric that compares elements from $\mathbf{X}$ and $\mathbf{Y}$, and $\mathcal{P}_p(p_1, p_2)$ represents the space of all partial permutation matrices, *i.e.*, matrices containing at most one "1" in each row or column.

Solving this integer optimisation problem is hard; Maciel and Costeira proposed a method that maps the integer optimisation problem to a dual problem on a continuous domain, where is can be solved efficiently using *concave programming* methods. If the metric J is linear, then this approach is guaranteed to find the globally optimal solution $\mathbf{P}^*$.

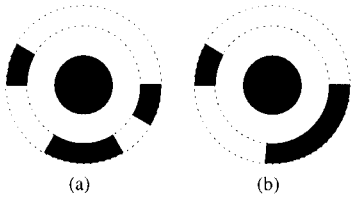

Figure 1: Sample fiducial patterns.

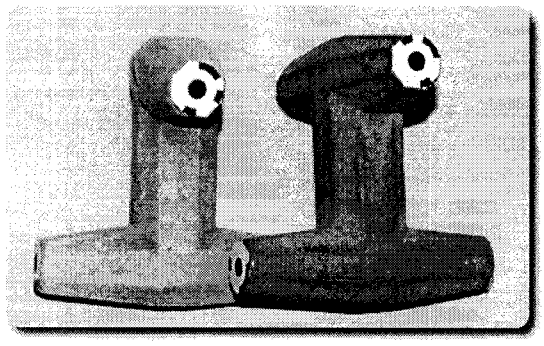

Figure 2: Sample image of two dolos models with various fiducial patterns attached.

3. System overview

Based on the literature presented in Section 2.1, a simplified circular fiducial pattern, roughly similar to the one proposed by López de Ipiña *et al.* [8] was selected. Figure 1 presents some examples of this fiducial pattern. This particular fiducial has a fairly large white ring between the central dot and the outer coding track to reduce aliasing problems when viewing the fiducial from a direction with an angle of more than 70° with respect to the surface normal.

These fiducials were scaled so that the diameter of the outer track was 7.1 mm in size to match the scale of the physical models, printed at 600 DPI using a standard laser printer, and fixed to the physical models as illustrated in Figure 2.

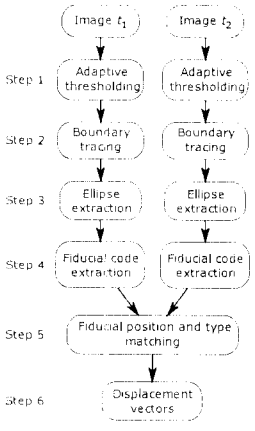

Figure 3: System overview

A system overview diagram is presented in Figure 3. The following algorithms were used to perform each of the steps:

1. The black regions in the image are identified by performing adaptive thresholding using the method of Bradley and Roth [11].
2. The pixel boundaries of objects are extracted using the component-labeling algorithm of Chang *et al.* [12]. Objects with very short boundaries (fewer than 10 pixels) or very long boundaries are discarded. This step produces all the boundaries of potential ellipses, corresponding to the central circle in the fiducial pattern.
3. Ellipse extraction is performed using the method of Ouellet and Hebert [13]. Note that the object boundaries extracted in step 2 are only used to seed the ellipse extraction algorithm; the algorithm derives ellipse parameters directly from the image gradient, producing significantly more accurate estimates of ellipse parameters compared to conventional algorithms. Objects that are unlikely to be ellipses are discarded by testing against conservative thresholds on various ellipse properties.
4. The fiducial code pattern is extracted by sampling the thresholded image along an elliptical path around the central dot of the candidate fiducial. The extracted signature is compared (using the Hamming distance metric) to a template library of known fiducial codes. Once a fiducial pattern is successfully identified, its fiducial code identifier and 3D coordinates are recorded. The 3D coordinates are determined directly from the ellipse parameters using the method proposed for the TRIP system [8].
5. The before-simulation (t_1) and after-simulation (t_2) images are processed with steps 1–5 to obtain the coordinates and identifiers of the fiducials in both images. The algorithm of Maciel and Costeira [10] is used to find the optimal association between fiducials from image t_1 and image t_2, producing as output the correspondence mapping.
6. Using the 3D coordinates of the fiducial patterns and the correspondence mapping, the displacement vectors of each of the matched fiducials is computed. For the purposes of this paper, the displacement vectors are merely visualised, but subsequent processing of the displacement vectors may be used to estimate the degree of damage to a breakwater armour unit array following a wave simulation.

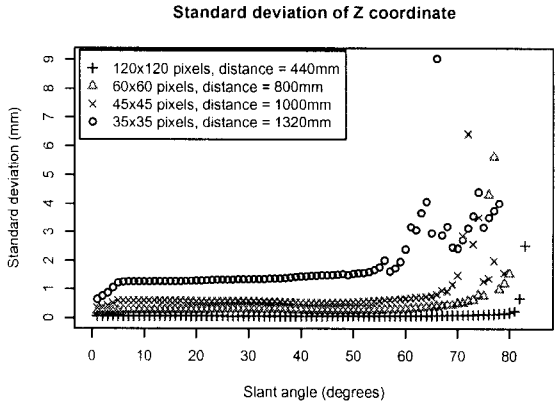

Figure 4: Standard deviation of z-coordinates, computed from degraded synthetic images (blur $\sigma = 0.5$, noise $\sigma = 1\%$).

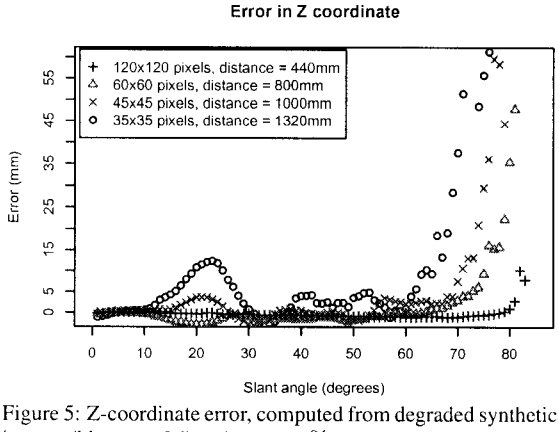

Figure 5: Z-coordinate error, computed from degraded synthetic images (blur $\sigma = 0.5$, noise $\sigma = 1\%$).

4. Performance evaluation of fiducials

The projection of a circle in world space onto the image plane is an ellipse, provided that a distortion-free pinhole camera model is assumed. A real lens will introduce some distortion, but because the lens distortion function typically varies slowly relative to the size of a fiducial, one can assume that the projection of a circle can be approximated with an ellipse.

A direct relationship exists between the imaged size of a fiducial, such as the one shown in Figure 1, and the accuracy with which its 3D position can be determined. The approximate ellipse formed by the boundary between the central black dot and the surrounding white ring is used to estimate the pose of the projected circle that it represents. Three factors directly influence the quality of this boundary ellipse: quantisation noise,

(a) 70° (b) 75° (c) 80°

Figure 6: Synthetic images, corresponding to the 35 × 35 pixel size experiment, magnified 500%. At this size, only (a) and (b) were successfully detected by the system.

Table 1: Maximum standard deviation (in mm), computed per slant angle, over slant angles $< 70°$, derived from degraded synthetic images.

Degradation (σ)		Fiducial size (pixels)			
Blur	Noise	120×120	60×60	45×45	35×35
0.5	1%	0.101	0.497	1.487	9.051
0.5	2%	0.203	0.989	2.059	5.991
0.7	1%	0.122	0.623	1.565	4.292
0.7	2%	0.245	1.238	2.378	7.907

Table 2: Maximum z-coordinate error (in mm) over slant angles $< 70°$, computed from degraded synthetic images.

Degradation (σ)		Fiducial size (pixels)			
Blur	Noise	120×120	60×60	45×45	35×35
0.5	1%	1.338	3.986	10.11	41.99
0.5	2%	1.534	5.042	11.42	46.08
0.7	1%	0.797	7.587	16.46	47.02
0.7	2%	1.037	8.902	18.42	52.55

sensor noise, and defocus blur.

Quantisation noise is effectively reduced by increasing the size of the ellipse, since more pixels now participate in its definition. Additive sensor noise is also effectively reduced by increasing the size of the ellipse, since the expected mean value of additive noise tends to zero as the number of pixels along the boundary of the ellipse increases. Defocus blur tends to spread the boundary over a larger area, ultimately leading to degradation owing to quantisation errors introduced by the limited bit depth of each pixel.

A monocular 3D pose approach is particularly sensitive to defocus blur, because this (together with quantisation) affects the apparent size of the ellipse, which in turn affects its estimated distance from the camera centre. The effect of the *slant angle*, that is, the angle between the surface normal of the fiducial and the viewing direction, should also be considered. Intuitively, as a circle turns away from the viewing direction, the eccentricity of its projection as an ellipse also increases, which effectively reduces the length of the boundary used to estimate the ellipse parameters, leading to larger errors in position estimates. In order to track displacements in the sub-millimeter range, the calculated position estimates must be repeatable, *i.e.*, their standard deviation over repeated measurements must be less than one millimeter.

4.1. Experiments using synthetic images

To evaluate the effect of these degradations on the proposed system, a number of experiments involving synthetic images were performed. For each viewing distance, a total of 90 base images are created using the POVRay ray tracer[1]. These base images correspond to fiducial patterns with slant angles from 0 to 90 degrees, in 1-degree increments. Each image was degraded first by blurring with a Gaussian kernel to simulate defocus, followed by the addition of zero-mean Gaussian noise to simulate sensor noise. For each viewing angle, distance and blur combination, a total of 30 additive noise images were instantiated. This process was repeated for several fiducial sizes, representing images captured at various distances from the target. Figure 6 illustrates some fiducial patterns viewed at large slant angles.

In a monocular 3D tracking system, it is expected that the extraction of the z-coordinate will be less reliable than the x- and y-coordinates. It is therefore important to measure the robustness of z-coordinate estimates on degraded images. Figure 4 illustrates the effects of slant angle and fiducial size on such degraded synthetic images. Observe how the z-coordinate standard deviation of the largest fiducial remains very small for slant angles less than 80°, whereas the smallest fiducial, at 35×35 pixels, produces significantly larger standard deviations, and degrades rapidly at slant angles greater than 55°. Table 1 lists the maximum standard deviation for a given target size at slant angles below 70° for various noise and blur combinations.

Similarly, Figure 5 and Table 2 illustrate the effective error in the z-coordinate under different slant angle and degradation combinations. The TRIP system [8] was reported to produce a z-coordinate error of 60mm at a slant angle of 60° at a distance of 1900mm, resulting in an error of 3.15% at the equivalent of a 35×35 pixel fiducial size. On the same size fiducial, our system achieves a maximum error of 14.7mm on slant angles below 60° at a distance of 1320mm, or 1.11% using degraded synthetic images[2] — see Figure 5. This indicates that the positional accuracy of the proposed system is comparable to that of the TRIP system.

The physical dolos models shown in Figure 2 measure around 38mm in length. From Table 2 one can see that the 60×60-pixel fiducial produces z-coordinate errors on the order of 10% of the size of the model at large slant angles. Fortunately, the x- and y-coordinate estimates are much more robust than the z-coordinate estimates. For comparison, the maximum Euclidean error (after discarding the z-coordinate) over all slant angles is only 0.0659mm for the values corresponding to row one of Table 2. This would suggest that a weighted Euclidean distance should be used when computing tracking the movement of a fiducial over time.

4.2. Experiments using captured images

In order to relate the synthetic results to real images captured with a digital camera, an experiment was set up to compare relative distances in both the real and synthetic images. Real images were captured using a 6-megapixel Nikon D40 camera at a focal length of 45mm. The images were captured in raw mode, and all the standard processing steps (such as sharpening) were disabled. The images were not corrected for lens distortion, since these effects are negligible in the central area of the lens used in these tests. The fiducials were imaged at distances ranging from 600mm to 900mm in 100mm increments. The diameter of the printed fiducials 7.1mm, to match the scale of the physical dolos models.

Figure 7 shows an image captured under the conditions used to evaluate the accuracy of distance measurements between fiducials. The combination of sensor noise, paper grain, and toner unevenness results in an estimated additive noise component of between 0.5% and 1% of the dynamic range. The same configuration was also modeled and rendered using POVRay. Table 3 lists mean distances measured between the fiducials, computed from a sample of 10 images at each camera-to-target distance. From the table one can see that the captured

[1] http://www.povray.org

[2] Our fiducial central dot is smaller, relative to the outer track, than the one used in TRIP. This accounts for the fact that the same size image, 35×35 pixels, results in different distances from the camera.

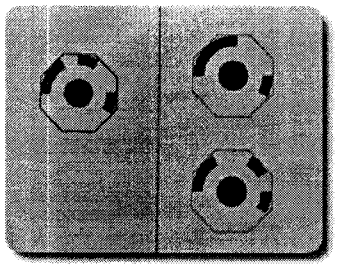

Figure 7: Fiducial test configuration image: the fiducial on the left ($\vec{v}_3$) is 25mm further from the camera than the two coplanar fiducials ($\vec{v}_1$, $\vec{v}_2$) on the right.

Table 3: Mean relative distance measures (and standard deviation) obtained from real and synthetic images. The matrix $\mathbf{P}$ denotes a projection onto the z-axis, and $\vec{v}_1$, $\vec{v}_2$ and $\vec{v}_3$ denote the 3D centre coordinates of three different fiducials. The expected values for the measures are 25mm and 10mm, respectively.

Camera	$\|\mathbf{P}\vec{v}_1 - \mathbf{P}\vec{v}_3\|$ (mm)		$\|\vec{v}_1 - \vec{v}_2\|$ (mm)	
distance (mm)	Real	Synth.	Real	Synth.
600	27.700	24.956	9.964	10.090
	(0.219)	(0.309)	(0.0187)	(0.0483)
700	24.272	23.633	10.043	10.043
	(0.441)	(0.328)	(0.0676)	(0.0057)
800	22.067	23.241	10.146	10.200
	(0.470)	(0.387)	(0.0790)	(0.0427)
900	21.474	23.992	10.464	10.107
	(0.965)	(0.549)	(0.1632)	(0.0301)

images ("Real") exhibit a slight trend, so that the z-distance between the fiducials appears to decrease as the camera moves further away from the fiducials. This effect can be partly attributed to the difficulty of obtaining the exact same focus quality at multiple camera-to-target distances — Table 2 clearly shows that increased blur, corresponding to poorer focus, leads to larger z-coordinate errors. The degraded synthetic images (produced with a blur σ of 0.5, and a noise σ of 1%) did not appear to suffer from this effect, as could be expected.

It is encouraging, to see that the standard deviation of z-distances captured at a distance of 800mm is less than 0.5mm. Distances measured between coplanar fiducials at the same distance from the camera appear to be much more robust, yielding an error of less than 0.2mm at a distance of 800mm, with a standard deviation of less than 0.08mm. From Table 3, it appears that a distance of 700mm offers sufficient accuracy to measure displacements on the order of 0.5mm with the camera specified above. Since these measurements were performed at a slant angle of 0°, it will still be necessary to filter fiducials with large slant angles, or to apply a weighted Euclidean metric to compensate for the large z-coordinate measurement errors that occur at large slant angles.

5. Application

The system described in Section 3 was used to track the movement of fiducials attached to physical breakwater armour unit models. For this experiment, the "dolos" type armour unit was selected, and four different fiducial patterns were attached to the four end-points of the dolos models. Note that the same four

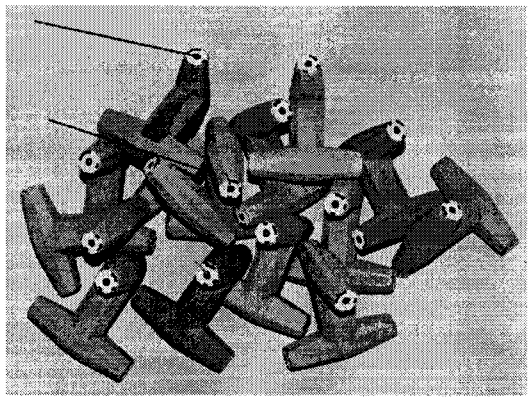

(a) Before movement, 50% cropped image

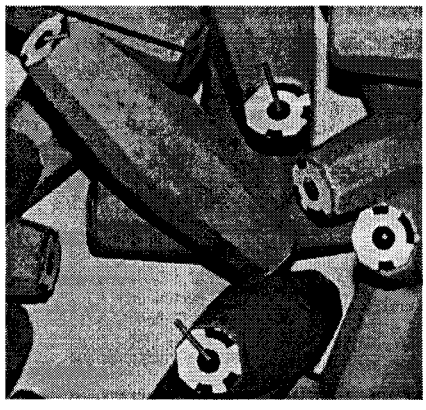

(b) Before movement, 5% cropped image

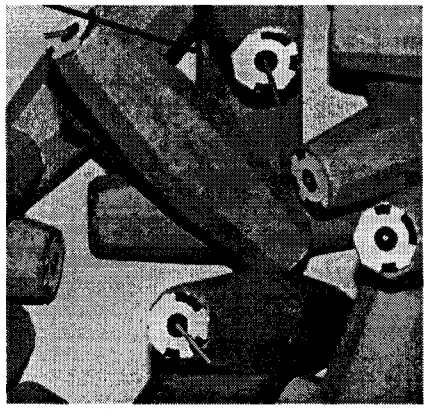

(c) After movement, 5% cropped image

Figure 8: Displacement vectors, calculated automatically by computing the movement of the fiducials between the two frames.

fiducial patterns were attached to all the dolosse, hence is it is not possible to uniquely identify a given dolos only by the code associated with its fiducial patterns. This method is at one extreme, where there are many objects with identical fiducials — it is possible to use more fiducial codes, but it may not be possible to assign unique fiducials to all the models in large simulations involving hundreds of dolosse. This experiment thus re-

lies heavily on correspondence matching to correctly track the movement of fiducials, and is therefore considered to be a more stringent test of the system.

An array of dolosse were arranged as shown in Figure 8(a). A number of dolosse were manipulated by hand to approximate the (hypothetical) movement induced by a wave-tank simulation. A second image was captured after the induced movement — a close-up of a region containing significant movement is shown in Figures 8(b) and (c). The green and red cylinders represent 3-dimensional displacement vectors. They were rendered using POVRay, and superimposed on top of the original images. Green cylinders represent a displacement of a matched pair of fiducials, *i.e.*, the exact same fiducial pattern occurred in the *before* and *after* images. Red cylinders indicate that the fiducial pattern types did not match, but that these are still likely candidates for a match, based on their physical proximity. For example, the two red cylinders visible in the upper left corner of Figure 8(a) are the result of the upper left-most dolos being displaced and overturned. This implied that the fiducials visible in the *before* image were facing away from the camera in the *after* image, but the correspondence algorithm still matched them with the fiducials on the reverse side of the model since they were still considered to be the most likely candidates.

Allowing matches between fiducials with different patterns can help to identify large displacements, but these matches are inherently less reliable than matches with identical patterns, and are only allowed here to illustrate the advantage of using a global correspondence matching algorithm.

If a large number of fiducial codes is used, then each individual dolos may receive its own code, unique within a certain radius in the original packing. This will reduce the possibility of incorrect matches to zero for most simulations.

6. Conclusions

This paper demonstrated that fiducials can used to track the movement of physical breakwater armour unit models to a sub-millimetre scale. The sensitivity and robustness of the system was investigated using both synthetic and captured images. Estimating the z-coordinate of a circular target using a monocular 3D system is feasible, but the accuracy and robustness of this estimate is heavily influenced by the size of the target, and the slant angle. On captured images, the absolute error in extracted x- and y-coordinates can be kept below 0.2mm; the absolute z-coordinate errors are on the order of 2–3mm, but with a standard deviation of less than 0.5mm.

The fiducial pattern used in our experiments depends on the central dot for the position calculations. In retrospect, this seems to have been a poor choice, since a different design, like that of Naimark and Foxlin [4], allows one to use the outer perimeter of the fiducial as circular reference. This would imply that the effective diameter of the circle would increase by a factor three, without increasing the physical size of the pattern. Even a more modest increase by a factor of two could reduce the position errors by a factor of three, as shown in Section 4. Future work will focus on repeating the experiments with an alternative fiducial design that maximises the size of the circle used to perform pose estimation.

7. Acknowledgements

The authors would like to thank the Strategic Research Panel (SRP) for providing support for this research through a CSIR project entitled "Advanced Digital Image Technology for Port Engineering".

8. References

[1] P. Bakker, A. van den Berge, R. Hakenberg, M. Klabbers, M. Muttray, B. Reedijk, and I. Rovers, "Development of Concrete Breakwater Armour Units," in *1st Coastal, Estuary and Offshore Engineering Specialty Conference of the Canadian Society for Civil Engineering*, New Brunswick, Canada, 2003.

[2] A. K. Cooper, J. M. Greben, F. van den Bergh, I. M. A. Gledhill, B. R. Cannoo, W. J. V. D. M. Steyn, and R. de Villiers, "A preliminary physics-engine model of dolosse interacting with one another," in *Proceedings of the Sixth South African Conference on Computational and Applied Mechanics (SACAM08)*, Cape Town, South Africa, March 2008.

[3] J. W. Berger, T. R. Patel, D. S. Shin, J. R. Piltz, and R. A. Stone, "Computerized stereochronoscopy and alternation flicker to detect optic nerve head contour change," *Ophthalmology*, vol. 107, no. 7, pp. 1316–1320, 2000.

[4] L. Naimark and E. Foxlin, "Circular data matrix fiducial system and robust image processing for a wearable vision-inertial self-tracker," in *Proceedings of the International Symposium on Mixed and Augmented Reality (ISMAR 2002)*, 2002, pp. 27–36.

[5] C. B. Bose and J. Amir, "Design of fiducials for accurate registration using machine vision," *IEEE Transactions on Pattern Analysis and Machine Intelligence*, vol. 12, no. 12, pp. 1196–1200, Dec 1990.

[6] C. B. Owen, F. Xiao, and P. Middlin, "What is the best fiducial," in *The First IEEE International Augmented Reality Toolkit Workshop*, Sept. 2002, pp. 98–105.

[7] J. Rekimoto and Y. Ayatsuka, "CyberCode: designing augmented reality environments with visual tags," in *Proceedings of DARE 2000 on Designing augmented reality environments*, Elsinore, Denmark, Apr. 2000, pp. 1–10.

[8] D. López de Ipiña, P. R. S. Mendonça, and A. Hopper, "TRIP: A Low-Cost Vision-Based Location System for Ubiquitous Computing," *Personal and Ubiquitous Computing*, vol. 6, no. 3, pp. 206–219, 2002.

[9] Z. Zhang, "Iterative point matching for registration of free-form curves and surfaces," *International Journal of Computer Vision*, vol. 13, no. 2, pp. 119–152, 1994.

[10] J. Maciel and J. P. Costeira, "A Global Solution to Sparse Correspondence Problems," *IEEE Transactions on Pattern Analysis and Machine Intelligence*, pp. 187–199, 2003.

[11] D. Bradley and G. Roth, "Adaptive Thresholding using the Integral Image," *Journal of Graphics Tools*, vol. 12, no. 2, pp. 13–21, 2007.

[12] F. Chang, C. J. Chen, and C. J. Lu, "A linear-time component-labeling algorithm using contour tracing technique," *Computer Vision and Image Understanding*, vol. 93, no. 2, pp. 206–220, 2004.

[13] J. N. Ouellet and P. Hebert, "A Simple Operator for Very Precise Estimation of Ellipses," in *Proceedings of the Fourth Canadian Conference on Computer and Robot Vision*, 2007, pp. 21–28.